nature chemistry

ARTICLES

PUBLISHED ONLINE: 14 APRIL 2013 | DOI: 10.1038/NCHEM.1621

Decoupling hydrogen and oxygen evolution during electrolytic water splitting using an electron-coupled-proton buffer

Mark D. Symes and Leroy Cronin*

Hydrogen is essential to several key industrial processes and could play a major role as an energy carrier in a future 'hydrogen economy'. Although the majority of the world's hydrogen supply currently comes from the reformation of fossil fuels, its generation from water using renewables-generated power could provide a hydrogen source without increasing atmospheric CO_2 levels. Conventional water electrolysis produces H_2 and O_2 simultaneously, such that these gases must be generated in separate spaces to prevent their mixing. Herein, using the polyoxometalate $H_3PMo_{12}O_{40}$, we introduce the concept of the electron-coupled-proton buffer (ECPB), whereby O_2 and H_2 can be produced at separate times during water electrolysis. This could have advantages in preventing gas mixing in the headspaces of high-pressure electrolysis cells, with implications for safety and electrolyser degradation. Furthermore, we demonstrate that temporally separated O_2 and H_2 production allows greater flexibility regarding the membranes and electrodes that can be used in water-splitting cells.

Total worldwide hydrogen production in 2011 exceeded 31 million metric tons[1], (>15.5 trillion moles), chiefly for use in the manufacture of ammonia (Haber–Bosch process) and in the petrochemical industries[2]. Moreover, hydrogen has attracted increasing attention recently as an energy carrier in its own right (the hydrogen economy), and in the synthesis of liquid fuels via catalytic hydrogenation of suitable substrates, such as CO_2 (refs 3,4). A major goal of these studies is to move away from using fossil fuels as the world's primary energy source, and instead to use renewables-generated power (for example, solar, hydro, wind and so on) to produce storable fuels[5–7]. However, >90% of the world's hydrogen is currently obtained by the reformation of fossil fuels[8,9], which increases the concentration of CO_2 in the atmosphere. The electrolysis of water to produce H_2 and O_2 (equations (1) and (2)) is an especially attractive alternative to reforming fossil fuels[10–12], because the starting material (water) is recovered when the hydrogen fuel is consumed (for example, in a fuel cell or by burning in air), and because the energy input required to electrolyse the water in the first place could be provided by renewable power sources. The oxygen-evolving reaction (OER) and the hydrogen-evolving reaction (HER) are given in equations (1) and (2):

$$H_2O \rightarrow \tfrac{1}{2}O_2 + 2H^+ + 2e^-, E_{oxidation} = -1.23\ V \quad (1)$$

$$2H^+ + 2e^- \rightarrow H_2, E_{reduction} = 0.0\ V \quad (2)$$

Water electrolysis may be performed under basic or acidic conditions[10], or at neutral pH[13]. Equations (1) and (2) hold under acidic conditions and describe the processes that occur in a proton exchange membrane electrolyser (PEME). The advantages of a PEME over a high pH alkaline electrolyser are increased current densities (up to $2\ A\ cm^{-2}$ for a PEME versus $\sim 0.2\ A\ cm^{-2}$ for a typical alkaline electrolyser), a wider possible range of power loadings (making PEMEs useful over a wider range of input powers) and faster power-up/power-down rates, which makes PEMEs highly responsive to changes in power input[14,15]. Moreover, PEMEs tend to be more efficient (and hence use less electricity per volume of hydrogen produced) than their alkaline counterparts[10]. These factors combine to make PEMEs ideally suited for applications in which the power input is variable in terms of magnitude and/or duration, such as the intermittent energy supplied by some renewable sources.

With regard to obtaining a hydrogen stream via water splitting that is essentially free of oxygen and of sufficient purity for use in industrial processes or in a fuel cell, systems in which O_2 and H_2 are created at separate points in space are currently essential. This is because, in traditional electrochemical cells, the OER and HER remain tightly coupled and therefore one half-reaction can only occur if the other also proceeds at an appreciable rate. This means that H_2 and O_2 are necessarily produced simultaneously, with the rate of one half-reaction explicitly dependent on the rate of the other. Natural photosynthetic systems that split water are able to separate the production of O_2 and H_2 equivalents in time as well as in space[16]. Similarly, some thermochemical cycles that rely on harsh reaction conditions may produce H_2 and O_2 from water at separate times on a large scale[17,18]. However, to our knowledge there exist no examples in the literature of a general and scalable electrolytic system that can separate the production of H_2 and O_2 in time.

Herein, we present an alternative approach to water splitting, whereby the electrons and protons generated during the oxidation of water to O_2 are taken up reversibly by an electron-coupled-proton buffer (ECPB), rather than being used directly to make H_2 (equation (3)). Subsequent reoxidation of the ECPB releases these protons and electrons for hydrogen production (equation (4)). Hence the ECPB acts as a reversible electron and proton donor/acceptor with a redox couple that is energetically intermediate between OER onset and HER onset. The overall result of using an ECPB is that H_2 and O_2 can be obtained from the electrolysis of water at completely different times; that is, the OER is completely decoupled from the HER to produce O_2 essentially free of H_2, and H_2 essentially free of O_2. In this way, two smaller energy inputs are used to split water to give H_2 and O_2

WestCHEM, School of Chemistry, The University of Glasgow, University Avenue, Glasgow G12 8QQ, UK. *e-mail: Lee.Cronin@glasgow.ac.uk

© 2013 Macmillan Publishers Limited. All rights reserved.

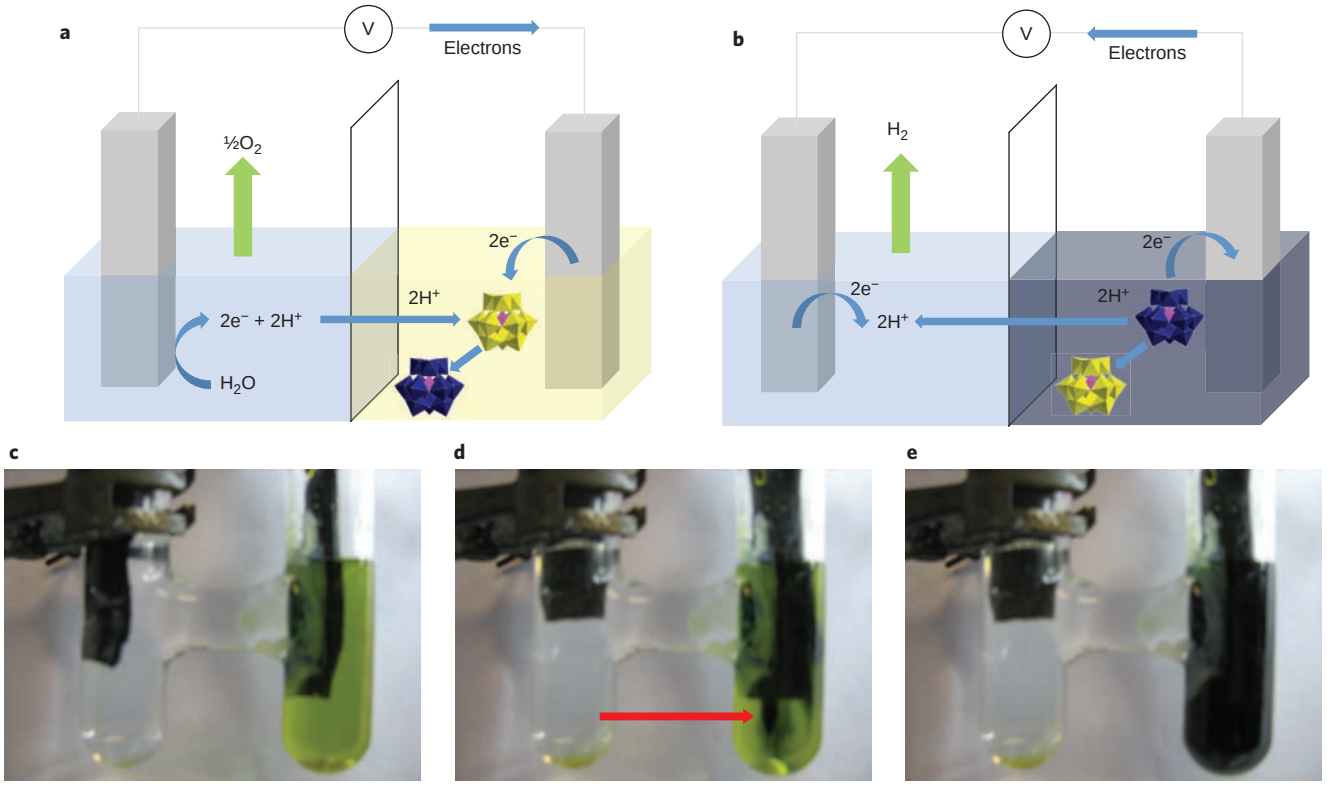

Figure 1 | Schematic of the ECPB-based approach to water splitting. a, Water is oxidized to give oxygen gas, protons and electrons. The electrons pass through the external circuit and the protons diffuse through the semipermeable membrane that separates the compartments. The ECPB in the other compartment is then reduced by the electrons and simultaneously accepts charge-balancing protons, turning from yellow to dark blue as it does so (V = the application of an external bias). **b**, Reoxidation of the ECPB releases protons, which can migrate through the membrane to the other electrode where they combine with the electrons removed from the ECPB to generate hydrogen gas. The ECPB returns to its original yellow colour as this happens. **c**, The ECPB in a cellulose-membrane electrolysis cell immediately after the start of reduction, showing the ECPB solution as bright yellow/green. **d**, After a few seconds, dark-blue reduced and protonated ECPB is visible near the cathode in the unstirred solution, indicated by the red arrow. **e**, After two minutes the entire ECPB solution turns dark blue (see Supplementary Fig. S16a–d for photographs of other cells).

at different times, as opposed to a single energy input that produces H_2 and O_2 simultaneously:

$$\mathrm{ECPB} + \mathrm{H_2O} \rightarrow [\mathrm{ECPB_{(two\text{-}electron\text{-}reduced)}}][\mathrm{H^+}]_2 + \tfrac{1}{2}\mathrm{O_2} \quad (3)$$

$$[\mathrm{ECPB_{(two\text{-}electron\text{-}reduced)}}][\mathrm{H^+}]_2 \rightarrow \mathrm{H_2} + \mathrm{ECPB} \quad (4)$$

We hypothesized that an ideal ECPB for water splitting would have the following properties: high solubility in water at room temperature (allowing high concentrations and hence a high storage capacity for protons and electrons), exist in a form in which the only countercation is H^+, consist only of earth-abundant elements, contain no easily oxidized moieties that might decompose during electrolysis, have at least one reversible redox wave between the onset of OER and HER, accept charge-balancing protons when it is reduced (hence it should buffer the solution pH during water splitting), be compositionally stable within the pH range studied and both the oxidized and reduced forms should be stable under ambient conditions on timescales that allow both of the steps shown in equations (3) and (4) to be completed. The ECPB chosen for this work was commercially available phosphomolybdic acid, which we show has all the attributes outlined above when used at a pH of 0.3, where it is compositionally stable[19] and exists primarily as the monoanion $(H_3O^+)[H_2PMo_{12}O_{40}]^-$ (see below). A general illustration of the ECPB approach is given in Fig. 1, which shows how the oxidation of water under an applied bias produces oxygen, protons and electrons. The protons and electrons are used to reduce and protonate reversibly the ECPB (Fig. 1a). Subsequent electrochemical reoxidation of the reduced ECPB (also under an applied bias) then releases the protons and electrons to give hydrogen at the other electrode (Fig. 1b).

Results

Redox potentials of the ECPB. The first reduced state of $(H_3O^+)[H_2PMo_{12}O_{40}]^-$ in aqueous solution is the two-electron reduced species $(H_3O^+)[H_4PMo_{12}O_{40}]^-$, for which the corresponding redox wave is highlighted with green arrows in Fig. 2[20,21]. The inset to Fig. 2 shows how the peak current for the anodic part of this wave varies with the square root of the scan rate: the linear trend observed indicates that this process involves solution-phase species under diffusion control.

To gauge the potentials required to produce a benchmark current density of 100 mA cm^{-2} for water splitting (with and without using an ECPB), we conducted controlled potential electrolysis with stirring on solutions of 1 M H_3PO_4 and 0.5 M phosphomolybdic acid, the results of which are shown in Fig. 3. To allow both oxidations and reductions of the ECPB to be performed in a general and technologically relevant fashion, a 50:50 mix of the oxidized and two-electron reduced species $(H_3O^+)[H_2PMo_{12}O_{40}]^-$ and $(H_3O^+)[H_4PMo_{12}O_{40}]^-$ (prepared by bulk electrolysis in either a two- or three-electrode configuration) was used. Figure 3a shows that to reduce this 50:50 ECPB solution at a current density of 100 mA cm^{-2}, a potential of +0.46 V (versus a normal hydrogen electrode (NHE)) is required, whereas a potential of −0.38 V is required to reduce protons to H_2 at a current density of

© 2013 Macmillan Publishers Limited. All rights reserved.

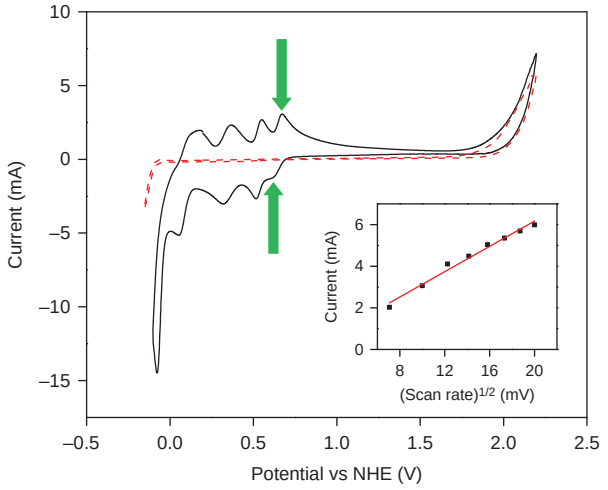

Figure 2 | Cyclic voltammograms showing the reversible redox waves of phosphomolybdic acid. Cyclic voltammograms of 0.5 M phosphomolybdic acid (solid black line) and 1 M H_3PO_4 (dashed red line) are shown. A three-electrode, single-compartment set-up was used, with a 2 mm diameter platinum disc working electrode, platinum mesh counter electrode and an Ag/AgCl reference electrode at a scan rate of 100 mV s^{-1}. The green arrows highlight the oxidation and reduction peaks associated with the first reduced state of phosphomolybdic acid. The inset shows a graph of the peak current versus square root of the scan rate for the reoxidation event associated with the first reversible two-electron wave (centred at +0.65 V) over the scan-rate range of 50–400 mV s^{-1}. The linear fit is provided as a guide to the eye. The error associated with the measurement of the currents was ±0.1 mA on each reading, which corresponds to the size of the data markers. All experiments were performed without degassing and under air.

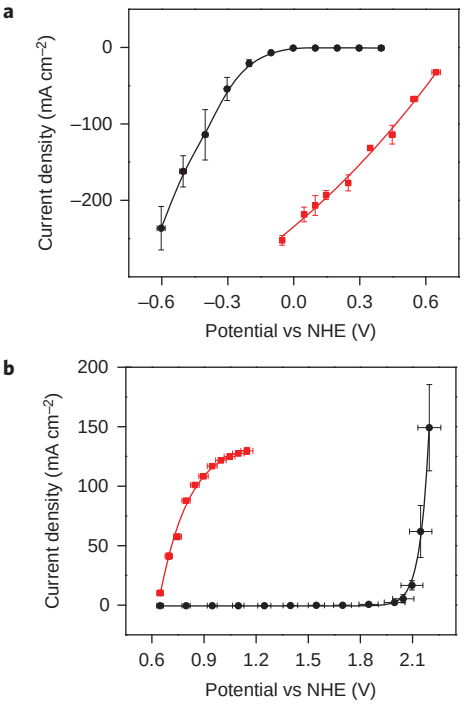

Figure 3 | Current–voltage curves obtained when stirring with and without an ECPB. a, Comparison of the reduction of a 0.5 M solution of 50:50 $(H_3O^+)[H_2PMo_{12}O_{40}]^-$ and $(H_3O^+)[H_4PMo_{12}O_{40}]^-$ (red) and a 1 M solution of H_3PO_4 (black). **b**, Comparison of the oxidation of a 0.5 M solution of 50:50 $(H_3O^+)[H_2PMo_{12}O_{40}]^-$ and $(H_3O^+)[H_4PMo_{12}O_{40}]^-$ (red) and a 1 M solution of H_3PO_4 (black). A three-electrode, single compartment set-up was used, with a 2 mm diameter platinum disc working electrode, platinum mesh counter electrode and an Ag/AgCl reference electrode, with *iR* compensation. Horizontal error bars correspond to the error associated with the *iR* compensation of the potentiostat (±3%) and the vertical error bars are based on the standard deviation of the currents from the mean current at that voltage.

100 mA cm^{-2}. Similarly, Fig. 3b shows that oxidation of the reduced ECPB proceeds at a current density of 100 mA cm^{-2} when the working electrode is poised at +0.85 V (versus NHE), whereas water oxidation to O_2 only reaches this current density when +2.17 V is applied. This allows us to quantify an expected energetic loss for the two-step system by adding up the relative terms. Hence, to reduce ECPB and oxidize water at 100 mA cm^{-2} requires $(+2.17 - +0.46) = 1.71$ V, and the reverse step (ECPB reoxidation and concomitant proton reduction) needs $(+0.85 - -0.38) = 1.23$ V. Therefore, the combined voltage required over the two steps is $1.71 + 1.23 = 2.94$ V. Meanwhile, single-step water splitting to perform the OER and HER together at 100 mA cm^{-2} requires $(+2.17 - -0.38) = 2.55$ V, which gives a maximum efficiency for the two-step process of 87% relative to the single-step process. As the use of a three-electrode configuration should minimize the effect of resistance on these metrics[22], we conclude that the majority of the 'extra' voltage required by the two-step system is because of the over-potential required to oxidize and reduce the ECPB at a current density of 100 mA cm^{-2} (that is, there is an energy penalty of around 400 mV for decoupling the OER and HER from each other under the conditions used here and at a current density of 100 mA cm^{-2}).

Using an ECPB to decouple the OER and HER. After establishing the energetics of phosphomolybdic acid as an ECPB using idealized three-electrode configurations, we proceeded to investigate electrolytic water splitting in the presence of an ECPB in a two-electrode set-up in which fixed potential differences were applied across the cell. Hence, one chamber of a two-compartment hydrogen cell was charged with 1 M H_3PO_4 and the other was filled with either a 0.5 M 50:50 mix of $(H_3O^+)[H_2PMo_{12}O_{40}]^-$ and $(H_3O^+)[H_4PMo_{12}O_{40}]^-$ in water, or 1 M H_3PO_4, depending on the process under investigation. The two compartments of the hydrogen cell were separated by a thin Nafion membrane, so that cations (in this case protons) could travel freely between the compartments, but the movement of anions across the membrane (especially the large ECPB anions) was greatly attenuated. In the ensuing discussion we define the electrode that is always in 1 M H_3PO_4 as the 'working' electrode, such that when a positive current is recorded this corresponds to water oxidation at this electrode (equation (1)) and, conversely, when the current is negative this corresponds to reduction of protons at this electrode (equation (2)).

Figure 4a shows how the current density for hydrogen evolution varied with the magnitude of the effective applied voltage, the composition of the electrodes and whether an ECPB was used or not. When a 0.5 M solution of 50:50 oxidized and two-electron reduced ECPB (the two-electron reduced ECPB may hereafter be termed ECPB*) was used in one compartment and both electrodes were platinum, potentials of more than −1 V across the cell gave increasingly large current densities, with bubbles evident on the working electrode (Fig. 4a, red line). By contrast, the black line in Fig. 4a shows the equivalent cell when both chambers were filled with 1 M H_3PO_4, that is using no ECPB. In this case, current onset was retarded significantly, and only became appreciable at voltages more negative than −2 V. This is because $(H_3O^+)[H_4PMo_{12}O_{40}]^-$ is easier to oxidize than water, and so when $(H_3O^+)[H_4PMo_{12}O_{40}]^-$ is available as an electron source, voltages significantly below that required to drive simultaneous O_2 and H_2 evolution can be used to generate hydrogen from aqueous solutions. Similarly, current densities for the OER improved significantly when oxidized ECPB was present in the other compartment of the cell (Fig. 4b).

© 2013 Macmillan Publishers Limited. All rights reserved.

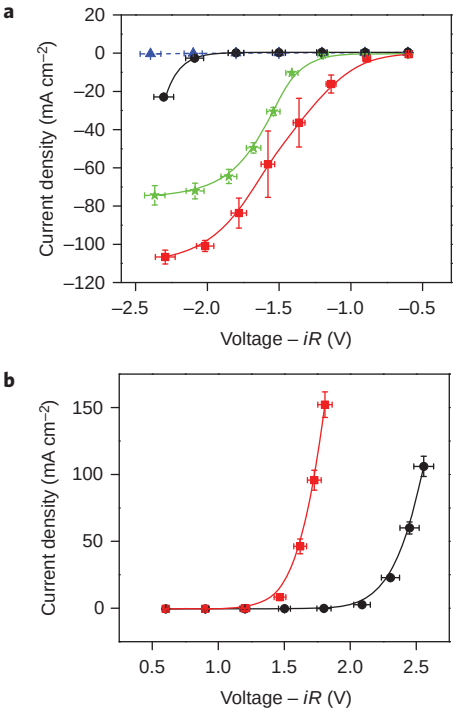

Figure 4 | Comparison of current densities for H_2 and O_2 evolution with and without the use of 0.5 M 50:50 $(H_3O^+)[H_2PMo_{12}O_{40}]^-$:$(H_3O^+)[H_4PMo_{12}O_{40}]^-$. a, Potential–current curves for the HER on platinum and carbon electrodes in a two-electrode configuration. For platinum, both electrodes were discs of area 0.031 cm^2 and for glassy carbon both electrodes were discs of area 0.071 cm^2. Red = platinum with ECPB, green = glassy carbon with ECPB, black = platinum without ECPB, blue = glassy carbon without ECPB. (The corresponding anodic half-reaction of this last process is electrode degradation and not oxidation of water[45].) The potential values reported are corrected for solution ohmic losses. **b**, Potential–current curves for the OER on platinum electrodes in a two-electrode configuration. Both electrodes were platinum discs of area 0.031 cm^2. Red = platinum with ECPB, black = platinum without ECPB. Horizontal error bars correspond to the error associated with the *iR* compensation of the potentiostat (±3%) and the vertical error bars are based on the standard deviation of the currents from the mean current at that voltage.

It is evident from Fig. 4 that the current densities that can be reached with an ECPB are limited by mass transport, which explains why the curves obtained using an ECPB tend to level off at high potentials. In an attempt to circumvent these mass-transport limitations, and to demonstrate low-voltage OER-decoupled hydrogen production using an ECPB, we substituted the small-area electrode in the ECPB solution by a larger area of platinum mesh or carbon cloth (chosen to reflect the nature of the small-area electrode that performs either the OER or HER). The results of this study for hydrogen production are shown in Fig. 5, in which current densities are normalized relative to the small-area electrode performing the HER (for a discussion of the OER in this cell at platinum electrodes, see Supplementary Section SI-7 and Fig. S3). The potential values that are reported in Fig. 5a were corrected for solution ohmic losses (*iR*). Potential–current curves for this data, which have not been corrected for ohmic losses, are given in Supplementary Fig. S4.

Moreover, it was found that employing easily oxidized ECPB* not only facilitated hydrogen production at low voltages from aqueous solutions, but also suppressed the OER at voltages where one-step water splitting to produce H_2 and O_2 simultaneously could theoretically occur. This was borne out by gas chromatography headspace analysis (GCHA), which showed that H_2 equivalent to 100% (±2%) of the charge passed (that is, full Faradaic efficiency, see Fig. 5b) was obtained when ECPB* was used in the counter-electrode compartment at an *iR*-corrected voltage[22] of −1.4 V (uncorrected voltage = −5 V, two-electrode set-up; see Supplementary Section SI-6 and Fig. S1 for details). However, the amount of O_2 generated under these conditions was below the detection limit of the GC system, which implies <0.4% of the O_2 production that would be expected if HER and OER occurred concurrently. Conversely, when the ECPB/ECPB* mixture was reduced electrochemically and water oxidized at the other (platinum) electrode, full Faradaic efficiency was observed for O_2 production but no H_2 was detected, which implies <0.1% of the expected H_2 production based on the amount of charge passed. Taken together, these results show that using an ECPB allows O_2 and H_2 to be produced at separate times during electrolytic water splitting.

Also shown in Figs 4a and 5a are *i*–*V* curves for the HER using two carbon electrodes. These figures show that when an ECPB is used (green curves), two carbon electrodes can simultaneously oxidize ECPB* to ECPB and reduce protons to H_2 at lower voltages than those required for two platinum electrodes to perform coupled O_2 and H_2 evolution without an ECPB (black curves). Both the

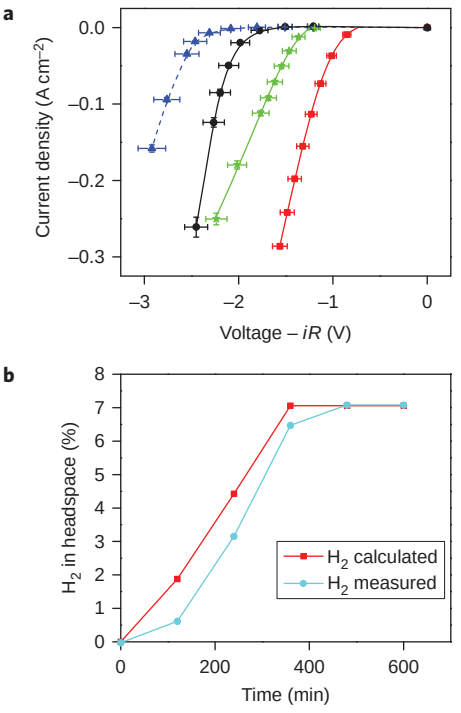

Figure 5 | Current densities and gas chromatography for H_2 evolution using an ECPB. a, Potential–current curves for platinum and carbon electrodes in a two-electrode configuration. For platinum, the electrode performing the HER had an area of 0.031 cm^2, and for glassy carbon the area was 0.071 cm^2. The counter electrodes were platinum mesh for the platinum experiments, and carbon felt for the carbon experiments. The counter electrode was placed in either 0.5 M ECPB/ECPB* or 1 M H_3PO_4. Red = platinum with ECPB, green = glassy carbon with ECPB, black = platinum without ECPB, blue = glassy carbon without ECPB. Error bars were determined as for Fig. 4. **b**, Representative trace of cumulative H_2 build-up in the headspace during HER on platinum electrodes. 'H_2 calculated' (red) was determined from the charge passed and 'H_2 measured' (blue) was determined by GC (Supplementary Section SI-6). The time lag between hydrogen production and detection by the GC resulted from the slow effusion of H_2 through the narrow tubing in the GC system. The error bars are within the data markers and correspond to ±2%.

© 2013 Macmillan Publishers Limited. All rights reserved.

carbon electrodes appeared unaltered after extended electrolysis in this configuration, and GCHA confirmed full Faradaic efficiency for H_2 generation under these conditions (Supplementary Fig. S5). Hence, provided a reduced, protonated ECPB is present in the counter-electrode compartment, two carbon electrodes can be used as stable and effective alternatives to platinum for rapid H_2 generation from aqueous solutions. Furthermore, it should be possible to interface this carbon hydrogen-production system with earth-abundant catalysts that are known to catalyse proton reduction at low pH[23–28].

Buffering capacity of the ECPB during electrolytic water splitting and comparison with those of other potential ECPBs. During the course of the foregoing experiments, the pH values of both the ECPB and H_3PO_4 solutions were found to be essentially invariant. Moreover, when H_3PO_4 was replaced with non-buffering HNO_3, the pH in both compartments also did not change (Supplementary Section SI-3), which suggests that as the ECPB was reduced at one electrode and water oxidized to O_2 and protons at the other, the ECPB acted to buffer the pH by storing both the protons and the electrons generated during water oxidation. This, in turn, suggests that the reduced and protonated ECPB exists in solution as the monoanion $(H_3O^+)[H_4PMo_{12}O_{40}]^-$, as the pH remained 0.3. However, not all polyoxometalates with appropriately positioned redox waves can act as ECPBs, which we show using the example of $Na_4(NH_4)_2[H_2VW_{17}O_{54}(VO_4)_2]$ (ref. 29; see also Supplementary Section SI-4). Similarly, 'redox mediators' that have reversible waves between the OER onset and HER onset have been used previously in photochemical systems known as artificial *Z*-schemes[30]. The Fe^{2+}/Fe^{3+} couple[31] and the I^-/IO_3^- couple[32,33] are the two most popular relays for this purpose; neither, however, is suitable for use as an ECPB. In the case of the I^-/IO_3^- couple, it is known that oxidation of the iodide does not lead cleanly to the iodate species, but rather forms mixtures of iodate and iodine, which can further react to give I_3^- species[33,34]. When we attempted to use NaI as an ECPB we found this to be problematic (Supplementary Section SI-11). The Fe^{2+}/Fe^{3+} couple is unsuitable as an ECPB on account of the small size of the ions (which means benzoylated cellulose membranes will not retain them in one side of the cell (see below)) and their positive charge (which means that the ions may permeate through Nafion membranes, which they are in any case known to attack[35]), and because Fe^{2+} salts are not stable in aqueous solution and tend to reoxidize spontaneously to Fe^{3+} salts (hence, aerial reoxidation of the Fe^{2+} would compete with electrochemical reoxidation, reducing yields of H_2). Phosphomolybdic acid, by contrast, does not suffer so significantly from these drawbacks.

Stability of the ECPB in the reduced and protonated form, and under cycling of the potential. $(H_3O^+)[H_2PMo_{12}O_{40}]^-$ could be reduced and reoxidized multiple times with little degradation being apparent (Supplementary Section SI-5). After two reduction–oxidation cycles, the reoxidized ECPB solution had an ultraviolet–visible (UV-vis) spectrum very similar to that of fresh $(H_3O^+)[H_2PMo_{12}O_{40}]^-$, which implies that <5% decomposition of the ECPB had occurred during cycling to the reduced and protonated form (Supplementary Fig. S2a–d). Samples of ECPB* were stored under air or under argon for various lengths of time before being reoxidized, and the charges that could be extracted from these samples were compared to the charges originally passed in reducing $(H_3O^+)[H_2PMo_{12}O_{40}]^-$ to ECPB*. When ECPB was reduced to ECPB* and then reoxidized to ECPB under air within three hours, 99.7% of the charge stored in ECPB* during water oxidation could be recovered. This fraction fell to 98% for a solution of ECPB* that was stirred in a container open to air for two weeks, and to 72% for a sample of ECPB* that was stored for eight months in a sealed container under air. Hence, over the time course of a few days, ECPB* is substantially stable with respect to spontaneous aerial oxidation, although the mechanism by which it slowly reoxidizes may be complex.

Regarding electrochemical stability, Supplementary Fig. S7 shows that a 500-cycle cyclic voltammogram of a 0.5 M solution of phosphomolybdic acid in water evinces no alterations in the shape or intensity of the spectrum. Similarly, a 0.5 M solution of the ECPB could be subjected to sequential bulk electrolysis over four reduction–oxidation cycles with <3% degradation (Supplementary Fig. S15a–c). Complementary analysis of samples of the ECPB in various charge states by mass spectrometry did not evince any irreversible speciation of the ECPB over the course of a two-electron reduction and reoxidization cycle (Supplementary Section SI-14 and Figs S11–S14)[36].

Efficiency of the ECPB system. The efficiency of an electrochemical system such as is described in this paper can be expressed as the ratio of the thermodynamic potential to the operating potential that was actually used. Equation (5) gives the chief factors that lead to efficiency losses (E_{loss}) as:

$$E_{loss} = \eta_{anode} + \eta_{cathode} + iR_{solvent} + E_{membrane} + E_{pH} \quad (5)$$

where η_{anode} and $\eta_{cathode}$ are the overpotentials at the anode and cathode, $iR_{solvent}$ is the potential loss associated with solution resistance, $E_{membrane}$ is the potential loss due to the membrane and E_{pH} is the potential loss that stems from the formation of pH gradients across the membrane[37]. The anodic and cathodic overpotentials can be reduced by employing catalysts on the electrodes. For example, the use of RuO_2 as an extremely effective anode for the OER could afford a current density of 0.1 A cm^{-1} (at room temperature and pH 1) at around +1.5 V versus NHE[38,39], which compares to a potential >2.1 V for the same current density on platinum (from Fig. 3b). Meanwhile, the resistance from the solution and membrane can be minimized by decreasing the distance between the electrodes and optimizing the membrane thickness. The E_{pH} term is more problematic (although the effects can be mitigated under very acidic conditions)[38], and equates to a loss of 59 mV per pH unit difference across the membrane, according to equation (6)[40]:

$$E_{pH} = (RT/F)\ln(10^{(pH_{cathode} - pH_{anode})}) \quad (6)$$

Hence, in our case E_{pH} is in the region of 36 mV, which is negligible in comparison to the size of the chief source of error, $iR_{solvent}$. In practice, as the Faradaic efficiencies for both oxygen evolution and hydrogen evolution are one, we obtain an overall efficiency of 79% for the two-step, two electrode configuration relative to the single-step process in which OER and HER remain coupled (see Supplementary Section SI-8 for details). This differs somewhat from the value of 87% efficiency found for a current density of 100 mA cm^{-2} (Fig. 3a,b) in a three-electrode configuration. We attribute this difference to residual uncorrected resistance in the two-electrode experiment, which will affect the two-step system twice as much as the one-step system. Future work will aim to increase the operational efficiency of the ECPB electrolyser by reducing $iR_{solvent}$ in particular.

Exploration of alternative membranes for water splitting using an ECPB. Phosphomolybdic acid is a comparatively large molecule (molecular mass (M_r) ~1,800, effective cross-sectional area ~1 nm^2)[41]. This, allied to the fact that an ECPB allows H_2 and O_2 production to be separated in time, means that pure H_2 and O_2 streams can be obtained from aqueous solutions using membranes that simply retain the ECPB in one compartment of

© 2013 Macmillan Publishers Limited. All rights reserved.

the cell. Thus, we replaced the Nafion membrane in our hydrogen cell with a commercially available benzoylated cellulose dialysis membrane, designed to separate molecules with $M_r > 1{,}200$. This membrane was found to be freely permeable to H_2 (Supplementary Section SI-9), yet proved effective at significantly retarding crossover of the large ECPB molecule (rate of crossover $< 1.5 \times 10^{-10}$ mol h^{-1}, measured by UV-vis spectroscopy over the time course of two weeks). Two-electrode current–potential analysis of a cell fitted with such a dialysis membrane and with carbon electrodes produced *i*–*V* curves almost identical to those obtained for the same electrode set with a Nafion separation membrane, which shows that cell performance was not impaired by replacing Nafion with cellulose (Supplementary Fig. S6).

As benzoylated cellulose is permeable to H_2, it was necessary to ascertain the behaviour of the oxidized ECPB to hydrogen. By bubbling with H_2 for two hours, we detected changes to both the cyclic voltammogram of the ECPB and some small growths in the UV-vis spectrum that are consistent with partial reduction of the ECPB (Supplementary Section SI-10 and Figs S9a–d and S10). This may imply that long-term storage of phosphomolybdic acid under a pure hydrogen atmosphere may not be appropriate. However, on shorter timescales, temporally separated OER and HER suggests that new types of membrane (that is, types that might not be as gas impermeable as Nafion), could potentially be considered for use in PEMEs. Alternatively, if Nafion membranes are employed, the ECPB could be used to mitigate against high-pressure O_2 and H_2 being produced simultaneously (the diffusion of H_2 and O_2 through Nafion at high temperature is one of the chief causes of degradation of such membranes)[42].

Discussion

In conclusion, we have introduced the concept of ECPBs that can reversibly store the protons and electrons produced during electrolytic water oxidation, thus breaking the voltage input necessary to split water into two. The ECPB we chose for this study was the polyoxometalate phosphomolybdic acid. However, numerous other compounds may be suitable for this role, provided that they are highly water soluble, can effectively buffer the pH during water splitting, have fully reversible and cyclable redox waves between OER and HER, are stable in both their oxidized and reduced forms, and do not cause degradation of other components within the cell (for example, electrodes and membranes). Using an ECPB, the OER is decoupled from the HER, which allows O_2 and H_2 to be produced separately in both space and time. This temporal separation allows greater flexibility in the type of membrane that may be used in acid-regime (photo)electrolysis cells, as gas impermeability is no longer a critical requisite for the production of pure H_2. Similarly, carbon electrodes can be used in combination with a reduced, protonated ECPB to generate hydrogen from aqueous solutions at current densities that rival those achieved with platinum electrodes in a non-ECPB cell, which raises the possibility of reducing precious-metal use in any technologically applicable device. The reduced and protonated ECPB need not necessarily be produced by direct water oxidation and routes for reduced ECPB production from sustainable fuel sources (such as biomass) could also be used[43,44]. Hence we believe that the use of ECPBs will create new possibilities in electrolyser design, opening up this engineering space to increased innovation. Further studies aimed at integrating catalysts for the OER and HER with this system, as well as identifying other ECPB systems that operate at different pH values and that have lower molecular weights, are currently underway in our laboratories.

Methods

Full experimental details for the ECPB stability tests, electrochemical procedures followed, results for cellulose-separated cells, electronic and mass spectra and GC headspace analyses are given in the Supplementary Information.

Received 31 October 2012; accepted 2 March 2013; published online 14 April 2013

References

1. US Department of Energy Hydrogen Analysis Resource Center, *Hydrogen Production, Worldwide and US Total Hydrogen Production*, http://hydrogen.pnl.gov/cocoon/morf/hydrogen/article/706 (2012).
2. Schrock, R. R. Reduction of dinitrogen. *Proc. Natl Acad. Sci. USA* **103,** 17087 (2006).
3. Armaroli, N. & Balzani, V. The hydrogen issue. *ChemSusChem* **4,** 21–36 (2011).
4. Olah, G. A., Prakash, G. K. S. & Goeppert, A. Anthropogenic chemical carbon cycle for a sustainable future. *J. Am. Chem. Soc.* **133,** 12881–12898 (2011).
5. Lewis, N. S. & Nocera, D. G. Powering the planet: chemical challenges in solar energy utilization. *Proc. Natl Acad. Sci. USA* **103,** 15729–15735 (2006).
6. Gust, D., Moore, T. A. & Moore, A. L. Solar fuels via artificial photosynthesis. *Acc. Chem. Res.* **42,** 1890–1898 (2009).
7. Cook, T. R. *et al.* Solar energy supply and storage for the legacy and nonlegacy worlds. *Chem. Rev.* **110,** 6474–6502 (2010).
8. Davis, S. J., Caldeira, K. & Matthews, H. D. Future CO_2 emissions and climate change from existing energy infrastructure. *Science* **329,** 1330–1333 (2010).
9. Häussinger, P., Lohmüller, R. & Watson, A. M. *Ullmann's Encyclopedia of Industrial Chemistry, Hydrogen, 2. Production* (Wiley-VCH, 2005).
10. Holladay, J. D., Hu, J., King, D. L. & Wang, Y. An overview of hydrogen production technologies. *Catal. Today* **139,** 244–260 (2009).
11. Walter, M. G. *et al.* Solar water splitting cells. *Chem. Rev.* **110,** 6446–6473 (2010).
12. Chen, X., Shen, S., Guo, L. & Mao, S. S. Semiconductor-based photocatalytic hydrogen generation. *Chem. Rev.* **110,** 6503–6570 (2010).
13. Kanan, M. W. & Nocera, D. G. *In situ* formation of an oxygen-evolving catalyst in neutral water containing phosphate and Co^{2+}. *Science* **321,** 1072–1075 (2008).
14. Atlam, O. An experimental and modelling study of a photovoltaic/proton-exchange membrane electrolyser system. *Int. J. Hydrogen Energy* **34,** 6589–6595 (2009).
15. Paul, B. & Andrews, J. Optimal coupling of PV arrays to PEM electrolysers in solar–hydrogen systems for remote area power supply. *Int. J. Hydrogen Energy* **33,** 490–498 (2008).
16. Barber, J. Photosynthetic energy conversion: natural and artificial. *Chem. Soc. Rev.* **38,** 185–196 (2009).
17. Funk, J. E. Thermochemical hydrogen production: past and present. *Int. J. Hydrogen Energy* **26,** 185–190 (2001).
18. Onuki, K., Kubo, S., Terada, A., Sakaba, N. & Hino, R. Thermochemical water-splitting cycle using iodine and sulfur. *Energy Environ. Sci.* **2,** 491–497 (2009).
19. Tsigdinos, G. A. Heteropoly compounds of molybdenum and tungsten. *Top. Curr. Chem.* **76,** 1–64 (1978).
20. Maeda, K., Himeno, S., Osakai, T., Saito, A. & Hori, T. A voltammetric study of Keggin-type heteropolymolybdate anions. *J. Electroanal. Chem.* **364,** 149–154 (1994).
21. Tanaka, N., Unoura, K. & Itabashi, E. Voltammetric and spectroelectrochemical studies of dodecamolybdophosphoric acid in aqueous and water–dioxane solutions at a gold-minigrid optically transparent thin-layer electrode. *Inorg. Chem.* **21,** 1662–1666 (1982).
22. Hamann, C. H., Hamnett, A. & Vielstich, W. *Electrochemistry* 2nd edn (Wiley-VCH, 2007).
23. Merki, D., Fierro, S., Vrubel, H. & Hu, X. Amorphous molybdenum sulfide films as catalysts for electrochemical hydrogen production in water. *Chem. Sci.* **2,** 1262–1267 (2011).
24. Le Goff, A. *et al.* From hydrogenases to noble metal–free catalytic nanomaterials for H_2 production and uptake. *Science* **326,** 1384–1387 (2009).
25. McKone, J. R. *et al.* Evaluation of Pt, Ni, and Ni–Mo electrocatalysts for hydrogen evolution on crystalline Si electrodes. *Energy Environ. Sci.* **4,** 3573–3583 (2011).
26. Chen, W-F. *et al.* Hydrogen-evolution catalysts based on non-noble metal nickel–molybdenum nitride nanosheets. *Angew. Chem. Int. Ed.* **51,** 6131–6135 (2012).
27. Merki, D., Vrubel, H., Rovelli, L., Fierro, S., & Hu, X. Fe, Co, and Ni ions promote the catalytic activity of amorphous molybdenum sulfide films for hydrogen evolution. *Chem. Sci.* **3,** 2515–2525 (2012).
28. Cobo, S. *et al.* A Janus cobalt-based catalytic material for electro-splitting of water. *Nature Mater.* **11,** 802–807 (2012).
29. Miras, H. N. *et al.* Exploring the structure and properties of transition metal templated $\{VM_{17}(VO_4)_2\}$ Dawson-like capsules. *Inorg. Chem.* **50,** 8384–8391 (2011).
30. Bard, A. J. Photoelectrochemistry and heterogeneous photo-catalysis at semiconductors. *J. Photochem.* **10,** 59–75 (1979).
31. Darwent, J. R. & Mills, A. Photo-oxidation of water sensitized by WO_3 powder. *J. Chem. Soc. Faraday Trans. 2* **78,** 359–367 (1982).

© 2013 Macmillan Publishers Limited. All rights reserved.

32. Abe, R., Sayama, K. & Sugihara, H. Development of new photocatalytic water splitting into H_2 and O_2 using two different semiconductor photocatalysts and a shuttle redox mediator IO_3^-/I^-. *J. Phys. Chem. B* **109,** 16052–16061 (2005).
33. Maeda, K., Higashi, M., Lu, D., Abe, R. & Domen, K. Efficient nonsacrificial water splitting through two-step photoexcitation by visible light using a modified oxynitride as a hydrogen evolution photocatalyst. *J. Am. Chem. Soc.* **132,** 5858–5868 (2010).
34. Skolnik, E. G. Compilation of site visit-based technical evaluations of hydrogen projects 1996–2001, Washington DC, http://www.osti.gov/bridge/servlets/purl/815055-bLCRmy/native/815055.pdf (2012).
35. Pozio, A., Silva, R. F., De Francesco, M. & Giorgi, L. Nafion degradation in PEFCs from end plate iron contamination. *Electrochim. Acta* **48,** 1543–1549 (2003).
36. Miras, H. N., Wilson, E. F. & Cronin, L. Unravelling the complexities of inorganic and supramolecular self-assembly in solution with electrospray and cryospray mass spectrometry. *Chem. Commun.* 1297–1311 (2009).
37. Hernández-Pagán, E. A. *et al.* Resistance and polarization losses in aqueous buffer-membrane electrolytes for water splitting photoelectrochemical cells. *Energy Environ. Sci.* **5,** 7582–7589 (2012).
38. Lodi, G., Sivieri, E., De Battisti, A. & Trasatti, S. Ruthenium dioxide-based film electrodes. III. Effect of chemical composition and surface morphology on oxygen evolution in acid solutions. *J. Appl. Electrochem.* **8,** 135–143 (1978).
39. Burke, L. D., Murphy, O. J., O'Neill, J. F. & Venkatesan, S. The oxygen electrode. Part 8. Oxygen evolution at ruthenium dioxide anodes. *J. Chem. Soc. Faraday Trans. 1* **73,** 1659–1671 (1977).
40. Sleutels, T. H. J. A., Hamelers, H. V. M., Rozendal, R. A. & Buisman, C. J. N. Ion transport resistance in microbial electrolysis cells with anion and cation exchange membranes. *Int. J. Hydrogen Energy* **34,** 3612–3620 (2009).
41. Himeno, S. & Takamoto, M. Difference in voltammetric properties between the Keggin-type $[XW_{12}O_{40}]^{n-}$ and $[XMo_{12}O_{40}]^{n-}$ complexes. *J. Electroanal. Chem.* **528,** 170–174 (2002).
42. Barbir, F. PEM electrolysis for production of hydrogen from renewable energy sources. *Solar Energy* **78,** 661–669 (2005).
43. Weinstock, I. A. *et al.* A new environmentally benign technology for transforming wood pulp into paper. Engineering polyoxometalates as catalysts for multiple processes. *J. Mol. Catal. A* **116,** 59–84 (1997).
44. Sonnen, D. M., Reiner, R. S., Atalla, R. H. & Weinstock, I. A. Degradation of pulp-mill effluent by oxygen and $Na_5[PV_2Mo_{10}O_{40}]$, a multipurpose delignification and wet air oxidation catalyst. *Ind. Eng. Chem. Res.* **36,** 4134–4142 (1997).
45. Engstrom, R. C. & Strasser, V. A. Characterization of electrochemically pretreated glassy carbon electrodes. *Anal. Chem.* **56,** 136–141 (1984).

Acknowledgements

This work was supported by the Engineering and Physical Sciences Research Council (UK) and Glasgow Solar Fuels. L.C. thanks the Royal Society/Wolfson Foundation for a Merit Award. M.D.S. thanks the University of Glasgow for a Lord Kelvin Adam Smith Research Fellowship. We are grateful to J. McIver (University of Glasgow) for assistance with the GC headspace analyses, H. N. Miras (University of Glasgow) for mass spectrometry and J. Liddell (University of Glasgow) for manufacturing numerous bespoke electrolysis cells.

Author contributions

M.D.S. and L.C. conceived the idea, planned experiments and co-wrote the paper, and M.D.S. performed the experiments and analysed the data.

Additional information

Supplementary information is available in the online version of the paper. Reprints and permissions information is available online at www.nature.com/reprints. Correspondence and requests for materials should be addressed to L.C.

Competing financial interests

The authors declare no competing financial interests.

© 2013 Macmillan Publishers Limited. All rights reserved.